IEEE Transactions on Automation Science and Engineering (T-ASE) paper, presented at ICRA 2026, Vienna, Austria.
Cite as T-ASE paper.

A Two-Stage Payload Dynamic Parameter Identification Method for Interactive Industrial Robots With Large Components

Mingxuan Liu, Pengcheng Li, Jinjun Duan, Lunqian Liu, Ye Shen, Wei Tian, and Yuqi Ji

***Abstract*—Taking human-robot collaborative assembly as an example, the methods based on contact forces can improve the assembly efficiency of industrial robots with large components in industrial manufacturing. However, due to the large size, high payload, assembly accuracy and dynamic changes in grip position, accurately estimating the contact forces between the payload and the operator becomes challenging when handling these large components. In this paper, a two-stage method is proposed for payload dynamic parameter identification. The parameter identification equation in the sensor coordinate system is initially established. Furthermore, the identification model of recursive restricted total least squares (RRTLS) based on total least squares (TLS) is constructed to achieve low-consumption online identification. According to the assembly requirements and payload characteristics, the posture coordinate system is designed for safety, including the feasible workspace for the robot. Subsequently, the static identification postures and dynamic excitation trajectory are planned to obtain static values and dynamic inertial parameters. In the end, a high-payload human-robot collaborative assembly system is built to validate the proposed method. Experimental results show that compared with the existing methods, the proposed approach can effectively identify and compensate the payload, leading to more accurate external force sensing.**

***Note to Practitioners*—Accurate payload parameter identification is essential for contact interactive applications of industrial robots. This research aims to solve two problems affecting parameter identification: the incompleteness of payload identification parameter consideration, and the real-time and security of large payload identification in industrial scenarios. In this paper, a two-stage payload dynamic parameter identification method is proposed, which can meet the application of large components in industrial scenarios. Firstly, a complete parameter identification model is established by decoupling the dynamic and static parameters. Then, a low-cost recursive identification is realized in a set feasible workspace. Finally, the external force sensing after parameter identification shows potential in but not limited to human-robot collaboration applications.**

***Index Terms*—Large components identification, inertial force/torque compensation, recursive restricted total least squares, contact force sensing, industrial robots.**

I. Introduction

IN RECENT years, the production process of the manufacturing industry has attached great importance to the application of human-robot collaborative assembly [1], [2]. Taking aircraft moving wings as an example, their vast size, weight, complex shape and assembly accuracy necessitate assembly methods and processes that differ from those for regular products. Manual installation not only has a high risk of collision, but also requires a significant amount of effort and strength to maintain the hoisting state manually. Human-robot collaborative assembly, which uses industrial robots to clamp payloads and interact with operators, combines the high load and high repeatability of robots with human flexibility. In this case, further combining with physical human-robot interaction methods such as position/force control [3], impedance control [4] or admittance control [5], flexible assembly tasks in unstructured environments can be rapidly implemented thereby improving assembly efficiency [6], [7], [8], [9]. In order to make the robot conform to human intention and achieve human-robot collaborative assembly, accurate sensing of forces generated by operator contact or environment collision is required.

The external force sensing methods of the robot end-effector are inevitably affected by the accuracy of robot parameters. Robot parameters include dynamic parameters and kinematic parameters. Model-based sensorless solutions [10], [11], [12] or joint torque sensor solutions [13], [14] must take into account the dynamics parameters of the entire robot structure (i.e. masses, inertia tensors, friction). Sensorless solutions use the motor current for estimation, which may not be accurate for industrial robots with high gear ratios and non-negligible friction effects [15], [16], [17]. Joint torque sensors

Received 29 August 2024; revised 21 January 2025; accepted 22 March 2025. Date of publication 2 April 2025; date of current version 24 April 2025. This article was recommended for publication by Associate Editor B. Lacevic and Editor P. Rocco upon evaluation of the reviewers' comments. This work was supported in part by the National Natural Science Foundation of China under Grant 52205530, Grant 52205017, and Grant U22A20204; and in part by the Civil Aerospace Technology Advance Research Project of the National Defense Administration of Science and Technology under Grant D020201. *(Corresponding authors: Pengcheng Li; Wei Tian.)*

Mingxuan Liu is with the College of Mechanical and Electrical Engineering, Nanjing University of Aeronautics and Astronautics, Nanjing 210016, China (e-mail: letmexx@nuaa.edu.cn).

Pengcheng Li, Jinjun Duan, and Wei Tian are with the College of Mechanical and Electrical Engineering, Nanjing University of Aeronautics and Astronautics, Nanjing 210016, China, and also with the State Key Laboratory of Intelligent Manufacturing System Technology for Complex Products, Beijing 100854, China (e-mail: lpccmee@nuaa.edu.cn; tw_nj@nuaa.edu.cn).

Lunqian Liu and Yuqi Ji are with Shanghai Aircraft Manufacturing Company, Shanghai 200120, China.

Ye Shen is with Shanghai Aerospace Electronic Technology Research Institute, Shanghai 201109, China.

This article has supplementary downloadable material available at https://doi.org/10.1109/TASE.2025.3557064, provided by the authors.

Digital Object Identifier 10.1109/TASE.2025.3557064

IEEE Transactions on Automation Science and Engineering (T-ASE) paper, presented at ICRA 2026, Vienna, Austria.

are often built into lightweight cobots and cannot be used in high-payload components [18], [19]. Indeed, for high-payload heterogeneous components in industrial scenarios, the above two methods are difficult to accurately obtain the dynamics parameters of the robot [20], [21]. The kinematic parameters of robots are often easy to obtain. For industrial robot applications, mounting a force/torque sensor at the end-effector is a feasible option [22], [23]. Combining the kinematics parameters of the robot, the identification of the inertia characteristics of the payload (i.e. mass, center of mass, inertia tensor) is a relevant solution to the contact force sensing [24], [25], [26].

For accurate contact force sensing, the identification of the inertial parameters of the payload is critical to eliminate the non-contact effects under the force/torque sensor. In the static situation, the measured values of the force/torque sensor include: the forces/torques generated by the payload gravity, the sensor zero-drift values, and the external contact forces/torques. The influence of payload gravity and sensor zero-drift values can be clarified by designing multiple postures in static situations and collecting corresponding data of 6 degrees of freedom (DOF) force/torque sensor [27]. In addition, the base inclination errors between the robot base coordinate system and the world coordinate system should also not be ignored [28]. In the dynamic situation, the inertial forces/torques of the payload, especially for high payloads, have a non-negligible impact on the data obtained by the 6-DOF force/torque sensor. A dynamic identification model has been established at [29] using the excitation trajectory for robot following and data acquisition, but the influence of inertial forces is neglected at low-speed trajectory. In [30], the optimized dynamic excitation trajectory is designed to identify the payload parameters. The non-contact influence caused by linear accelerations is also considered in the inertial force compensation component. To compensate for inertial forces caused by angular velocities/accelerations and inertial tensor, the effects of each relevant inertial parameter are decoupled by executing specific test motions [31].

The most common method for off-line or batch dynamic parameter identification is the identification model using ordinary least squares (LS) estimation [29], [30]. The LS method and its variants, including weighted least squares [32] and double weighted least squares [33], are easy to implement but lack noise immunity. The data matrix contains multiple parameter errors, including kinematic parameters and measured force/torque. Considering the influence of covariance in the LS identification matrix, the accuracy of parameter identification can be further improved. To solve this problem, a better recursive total least squares (RTLS) method is proposed compared with recursive least squares and recursive instrument variables. [34], [35], [36].

The design of identification postures and excitation trajectories for careful planning can effectively stimulate the identification parameters. In the case of the unknown transition between the force/torque sensor and the robot, [37] proposes the rotation calibration to realize bias estimation. The fifth-order polynomial trajectory in the joint space is proposed as the excitation trajectory in [38]. To produce repeatable identification trials, periodic excitation trajectories based on the Fourier series or modified Fourier series have been proposed [39]. The design of excitation trajectories is continuously optimized by new computationally efficient and intuitive optimality criterion [40]. Furthermore, the safety of excitation trajectories in the identification process is also emphasized [31].

As mentioned above, static and dynamic identification have different discernible parameters. The static identification will ignore the dynamic parameters such as the inertia tensor, which have a great influence on large components, while the dynamic identification cannot obtain accurate specific static parameters, such as the sensor zero-drift values and the base inclination errors. The proposed two-step method takes full account of the identification parameters by combining the two methods. This combination contributes to rapid and heterogeneous assembly requirements in industrial scenarios. The identification and compensation of the payload attached to the robot end-effector are affected by multi-source factors, making accurate external force sensing problematic. The previous methods have achieved relatively good force sensing results due to the consideration of certain factors, but they are confined to tiny and light experimental components (payload less than 5 kg, length less than 50 cm). As the payload and length increases:

- Sensor noise and external forces to be overcome by the operator will increase. The identification parameters should be fully considered to reduce the identification error.
- During the identification process, the trajectories or postures of large components need to be planned more carefully for safety.

According to the characteristics of large components, a two-stage method is proposed to comprehensively consider the relevant factors in parameter identification. A RRTLS identification model is designed to achieve low computational cost online identification. With safety in mind, identification postures and excitation trajectories are also designed in feasible workspace. The main contributions of this work can be summarized as follows:

- Propose a payload identification method with comprehensive parameter consideration for interactive industrial robots with large components, filling a gap in this area of research.
- Introduce a RRTLS algorithm with low computational cost and suitable for online updating to meet the requirements of real-time recursive computing in industrial scenarios.
- Design a feasible workspace and plan the identification postures and excitation trajectory in the space to meet the safety requirements in the actual scene.
- Carry out experiments on a human-robot collaborative assembly platform, and the experimental results combined with secondary zero-drift compensation show its potential in but not limited to human-robot collaborative applications.

IEEE Transactions on Automation Science and Engineering (T-ASE) paper, presented at ICRA 2026, Vienna, Austria.

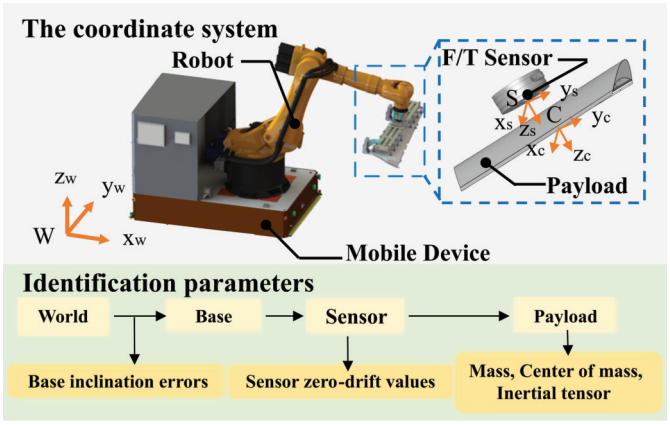

Fig. 1. Identification parameters are distributed among multiple coordinate systems.

In this paper, A two-stage payload dynamic parameter identification method is proposed to solve the external force sensing of large components. The paper proceeds as follows: In the Section II, the identification equations of static/dynamic parameters in the sensor frame are established based on the Newton-Euler method. The parameter identification model based on the RRTLS method is constructed in the Section III. The Section IV designs identification postures and excitation trajectories. In Section V, the experiments and experimental results analysis are presented. Finally, the conclusion is presented in Section VI.

II. Problem Formulation

This section analyzes the components of the raw data measured by the force/torque sensor and establishes the relationship equation between the relevant forces/torques and the parameters to be identified under dynamic and static conditions.

The identification parameters in the coordinate system are illustrated in Fig. 1. {W} represents the world coordinate system. {B} represents the base coordinate system of the robot installed on the mobile device. {S} represents the force/torque sensor coordinate system. The axes of the payload coordinate system {C} are parallel to the axes of {S}.

The 6-DOF forces/torques measured by the force/torque sensor are represented as:

$$\boldsymbol{F}_{raw} = \boldsymbol{F}_{nc} + \boldsymbol{F}_0 + \boldsymbol{F}_{ext} \tag{1}$$

where $\boldsymbol{F}_{raw} = [f_x, f_y, f_z, \tau_x, \tau_y, \tau_z]^T \in \mathbb{R}^{6\times1}$ is the raw data measured by the force/torque sensor. $\boldsymbol{F}_{nc} = [\boldsymbol{f}_{nc}, \boldsymbol{\tau}_{nc}]^T \in \mathbb{R}^{6\times1}$, where $\boldsymbol{f}_{nc}$ and $\boldsymbol{\tau}_{nc}^T$ represents the non-contact 3-DOF forces and torques caused by gravity and inertia of the payload, respectively. $\boldsymbol{F}_0 = [f_{x0}, f_{y0}, f_{z0}, \tau_{x0}, \tau_{y0}, \tau_{z0}]^T \in \mathbb{R}^{6\times1}$ denotes the sensor zero-drift values. $\boldsymbol{F}_{ext} \in \mathbb{R}^{6\times1}$ is external contact forces/torques.

A. Dynamic Identification Equation

To estimate the inertial parameters of the payload, the dynamic identification equation based on the Newton-Euler approach relating the non-contact forces/torques and payload velocities and accelerations is as [41] and [42]

$$\begin{bmatrix} {}^S\boldsymbol{f}_{nc} \\ {}^S\boldsymbol{\tau}_{nc} \end{bmatrix} = \begin{bmatrix} m{}^S\boldsymbol{a} + m{}^S\boldsymbol{g} + {}^S\boldsymbol{\alpha} \times m{}^S\boldsymbol{c} + {}^S\boldsymbol{\omega} \times ({}^S\boldsymbol{\omega} \times m{}^S\boldsymbol{c}) \\ {}^S\boldsymbol{I}{}^S\boldsymbol{\alpha} + {}^S\boldsymbol{\omega} \times ({}^S\boldsymbol{I}{}^S\boldsymbol{\omega}) + m{}^S\boldsymbol{c} \times {}^S\boldsymbol{a} + m{}^S\boldsymbol{c} \times {}^S\boldsymbol{g} \end{bmatrix} \tag{2}$$

where

$$\boldsymbol{I} = \begin{bmatrix} I_{xx} & I_{xy} & I_{xz} \\ I_{yx} & I_{yy} & I_{yz} \\ I_{zx} & I_{zy} & I_{zz} \end{bmatrix} \tag{3}$$

and m is the mass of the payload. ${}^S\boldsymbol{a}$ and ${}^S\boldsymbol{\alpha}$ denote linear and angular accelerations respectively. ${}^S\boldsymbol{\omega}$ are the angular velocities, ${}^S\boldsymbol{g} = [{}^Sg_x, {}^Sg_y, {}^Sg_z]^T$ is the gravity vector, ${}^S\boldsymbol{c} = [{}^Sc_x, {}^Sc_y, {}^Sc_z]^T$ is the center of mass, ${}^S\boldsymbol{I}$ represents the inertial tensor matrix. All variables are represented in {S}. Eq.(2) can be reformulated to indicate the linear relationship between ${}^S\boldsymbol{F}_{nc}$ and the inertial parameter vector ${}^S\boldsymbol{\Phi} = [m, m{}^Sc_x, m{}^Sc_y, m{}^Sc_z, {}^SI_{xx}, {}^SI_{xy}, {}^SI_{xz}, {}^SI_{yy}, {}^SI_{yz}, {}^SI_{zz}]^T$

$${}^S\boldsymbol{F}_{nc} = {}^S\boldsymbol{A}({}^S\boldsymbol{a}, {}^S\boldsymbol{\alpha}, {}^S\boldsymbol{\omega}, {}^S\boldsymbol{g}){}^S\boldsymbol{\Phi} \tag{4}$$

The data matrix ${}^S\boldsymbol{A}$ is given in Eq.(5), as shown at the bottom of the page, and the index ^{S} is omitted.

B. Static Identification Equation

When the robot is installed on the mobile device, the flatness deviation between {B} and {W} often exists due to the leveling error of the mobile device or the uneven ground. This error leads to an angle offset of the Z-axis of {B} from the gravity vector in {W}. The base inclination errors of {B} and {W} on the X-axis and Y-axis are represented by U and V respectively, then the rotation matrix of {B} relative to {W} satisfies:

$${}^W_BR = \begin{bmatrix} 1 & 0 & 0 \\ 0 & cosU & -sinU \\ 0 & sinU & cosU \end{bmatrix} \begin{bmatrix} cosV & 0 & sinV \\ 0 & 1 & 0 \\ -sinV & 0 & cosV \end{bmatrix} \tag{6}$$

The rotation matrix of {S}, which is the same as the robot tool coordinate frame, relative to {B} is shown in Eq.(7), at the bottom of the next page. The Z-Y-X Euler angles of {S} with respect to {B} are expressed by $(\gamma_z, \gamma_y, \gamma_x)$.

The unit vector of the gravity vector in the negative direction of the Z-axis in {W} is

$${}^W\hat{\boldsymbol{g}} = \begin{bmatrix} 0 \\ 0 \\ -1 \end{bmatrix} \tag{8}$$

$${}^S\boldsymbol{A} = \begin{bmatrix} a_x + g_x & -\omega_y^2 - \omega_z^2 & \omega_x\omega_y - \alpha_z & \omega_x\omega_z - \alpha_y & 0 & 0 & 0 & 0 & 0 & 0 \\ a_y + g_y & \omega_x\omega_y + \alpha_z & -\omega_x^2 - \omega_z^2 & \omega_y\omega_z - \alpha_x & 0 & 0 & 0 & 0 & 0 & 0 \\ a_z + g_z & \omega_x\omega_z - \alpha_y & \omega_y\omega_z + \alpha_x & -\omega_y^2 - \omega_x^2 & 0 & 0 & 0 & 0 & 0 & 0 \\ 0 & 0 & a_z + g_z & -a_y - g_y & \alpha_x & \alpha_y - \omega_x\omega_z & \alpha_z + \omega_x\omega_y & -\omega_y\omega_z & \omega_y^2 - \omega_z^2 & \omega_y\omega_z \\ 0 & -a_z - g_z & 0 & a_x + g_x & \omega_x\omega_z & \alpha_x + \omega_y\omega_z & \omega_z^2 - \omega_x^2 & \alpha_y & \alpha_z - \omega_x\omega_y & -\omega_x\omega_z \\ 0 & a_y + g_y & -a_x - g_x & 0 & -\omega_x\omega_y & \omega_x^2 - \omega_y^2 & \alpha_x - \omega_y\omega_z & \omega_x\omega_y & \alpha_y + \omega_x\omega_z & \alpha_z \end{bmatrix} \tag{5}$$

IEEE Transactions on Automation Science and Engineering (T-ASE) paper, presented at ICRA 2026, Vienna, Austria.

The unit vector of the gravity vector in {S} is

$$ {}^{S}\hat{\boldsymbol{g}} = {}^{S}_{B}R^{B}_{W}R^{W}\hat{\boldsymbol{g}} = {}^{B}_{S}R^{T}\,{}^{W}_{B}R^{T}\,{}^{W}\hat{\boldsymbol{g}} = {}^{B}_{S}R^{T}\begin{bmatrix}\cos U \sin V\\ -\sin U\\ -\cos U\cos V\end{bmatrix} \tag{9}$$

Then the gravity vector in {S} is

$$ {}^{S}\boldsymbol{g} = {}^{S}\hat{\boldsymbol{g}}g_{con} = {}^{B}_{S}R^{T}\begin{bmatrix}g_{con}\cos U\sin V\\ -g_{con}\sin U\\ -g_{con}\cos U\cos V\end{bmatrix} = \begin{bmatrix}{}^{S}g_x\\ {}^{S}g_y\\ {}^{S}g_z\end{bmatrix} \tag{10}$$

where g_{con} is the gravitational constant.

Furthermore, to obtain $\boldsymbol{F}_{nc}$, it is necessary to eliminate the sensor zero-drift values from the raw data measured by the force/torque sensor, that is, the time-varying drifts in the strain-gauge force/torque sensor.

When the robot is motionless without external contact forces, the combination of Eq.(1) and Eq.(2) yields

$$\begin{cases} {}^{S}f_x = m{}^{S}g_x + {}^{S}f_{x0}\\ {}^{S}f_y = m{}^{S}g_y + {}^{S}f_{y0}\\ {}^{S}f_z = m{}^{S}g_z + {}^{S}f_{z0}\end{cases} \tag{11}$$

$$\begin{cases} {}^{S}\tau_x = m{}^{S}g_z{}^{S}c_y - m{}^{S}g_y{}^{S}c_z + {}^{S}\tau_{x0}\\ {}^{S}\tau_y = m{}^{S}g_x{}^{S}c_z - m{}^{S}g_z{}^{S}c_x + {}^{S}\tau_{y0}\\ {}^{S}\tau_z = m{}^{S}g_y{}^{S}c_x - m{}^{S}g_x{}^{S}c_y + {}^{S}\tau_{z0}\end{cases} \tag{12}$$

Substitute Eq.(10) into Eq.(11)

$$\begin{bmatrix}{}^{S}f_x\\ {}^{S}f_y\\ {}^{S}f_z\end{bmatrix} = \left[{}^{B}_{S}R^{T} \mid I_3\right]_{3\times 6}\begin{bmatrix}\kappa_x\\ \kappa_y\\ \kappa_z\\ {}^{S}f_{x0}\\ {}^{S}f_{y0}\\ {}^{S}f_{z0}\end{bmatrix} \tag{13}$$

where

$$\begin{bmatrix}\kappa_x\\ \kappa_y\\ \kappa_z\end{bmatrix} = \begin{bmatrix}mg_{con}\cos U\sin V\\ -mg_{con}\sin U\\ -mg_{con}\cos U\cos V\end{bmatrix} \tag{14}$$

Substitute Eq.(11) into Eq.(12)

$$\begin{bmatrix}{}^{S}\tau_x\\ {}^{S}\tau_y\\ {}^{S}\tau_z\end{bmatrix} = \begin{bmatrix}0 & {}^{S}f_z & -{}^{S}f_y & 1 & 0 & 0\\ -{}^{S}f_z & 0 & {}^{S}f_x & 0 & 1 & 0\\ {}^{S}f_y & -{}^{S}f_x & 0 & 0 & 0 & 1\end{bmatrix}\begin{bmatrix}{}^{S}c_x\\ {}^{S}c_y\\ {}^{S}c_z\\ \iota_1\\ \iota_2\\ \iota_3\end{bmatrix} \tag{15}$$

where

$$\begin{bmatrix}\iota_1\\ \iota_2\\ \iota_2\end{bmatrix} = \begin{bmatrix}{}^{S}\tau_{x0} + {}^{S}f_{y0}\times{}^{S}c_z - {}^{S}f_{z0}\times{}^{S}c_y\\ {}^{S}\tau_{y0} + {}^{S}f_{z0}\times{}^{S}c_x - {}^{S}f_{x0}\times{}^{S}c_z\\ {}^{S}\tau_{z0} + {}^{S}f_{x0}\times{}^{S}c_y - {}^{S}f_{z0}\times{}^{S}c_x\end{bmatrix} \tag{16}$$

By combining Eq.(13) and Eq.(15), the static identification equation representing the relationship between $\boldsymbol{F}_{raw}$ and base inclination errors and the zero-drift values in {S} can be obtained as

$$ {}^{S}\boldsymbol{F}_{raw} = {}^{S}\boldsymbol{B}(\gamma_z,\gamma_y,\gamma_x,{}^{S}f_x,{}^{S}f_y,{}^{S}f_z){}^{S}\boldsymbol{\Psi} \tag{17}$$

where

$$ {}^{S}\boldsymbol{\Psi} = \left[\kappa_x,\kappa_y,\kappa_z,{}^{S}f_{x0},{}^{S}f_{y0},{}^{S}f_{z0},{}^{S}c_x,{}^{S}c_y,{}^{S}c_z,\iota_1,\iota_2,\iota_3\right]^{T} \tag{18}$$

By bringing the relevant parameters of Eq.(18) into Eq.(14) and Eq.(16), base inclination errors and zero-drift values of three orthogonal torques can be obtained as

$$\begin{bmatrix}U\\ V\end{bmatrix} = \begin{bmatrix}\arcsin\left(\dfrac{\kappa_y}{\sqrt{\kappa_x^2+\kappa_y^2+\kappa_z^2}}\right)\\ \arctan\left(\dfrac{\kappa_x}{\kappa_z}\right)\end{bmatrix} \tag{19}$$

and

$$\begin{bmatrix}{}^{S}\tau_{x0}\\ {}^{S}\tau_{y0}\\ {}^{S}\tau_{z0}\end{bmatrix} = \begin{bmatrix}\iota_1 - {}^{S}f_{y0}\times{}^{S}c_z + {}^{S}f_{z0}\times{}^{S}c_y\\ \iota_2 - {}^{S}f_{z0}\times{}^{S}c_x + {}^{S}f_{x0}\times{}^{S}c_z\\ \iota_3 - {}^{S}f_{x0}\times{}^{S}c_y + {}^{S}f_{y0}\times{}^{S}c_x\end{bmatrix} \tag{20}$$

The dynamic parameter identification equation only considers the forces/torques caused by the payload gravity and inertia. The neglected base inclination errors and sensor zero-drift values can be further corrected by the static identification equation.

III. Parameter Identification Method

This section analyzes the defects of the standard LS error model and then introduces the RRTLS identification method based on the TLS error model.

A. Error Model of TLS Identification

Suppose a set of linear equations to be estimated

$$\mathcal{M} \approx \mathcal{N}\mathcal{X} \tag{21}$$

where $\mathcal{M}$ represents the matrix of measured outputs, $\mathcal{N}$ represents the matrix that contains the measured inputs, and $\mathcal{X}$ represents the parameter vector. Standard LS is based on the assumption that $\mathcal{N}$ is free of errors. The errors are modeled as an additive vector $\widetilde{\mathcal{M}}$ of $\mathcal{M}$. Therefore, the variable error model of the LS method is given as

$$\overline{\mathcal{M}} + \widetilde{\mathcal{M}} = \mathcal{N}\mathcal{X}, \mathcal{M} = \overline{\mathcal{M}} + \widetilde{\mathcal{M}} \tag{22}$$

where $\overline{\mathcal{M}}$ represents the true output matrix.

For the static/dynamic identification equation in this paper, the LS error model is inadequate for the consideration of noise in the data matrices $\boldsymbol{A}$ or $\boldsymbol{B}$ during the identification of inertial parameters. The TLS method is based on a more

$$ {}^{B}_{S}R = R_Z(\gamma_z)R_Y(\gamma_y)R_X(\gamma_x) = \begin{bmatrix}cos\gamma_z & -sin\gamma_z & 0\\ sin\gamma_z & cos\gamma_z & 0\\ 0 & 0 & 1\end{bmatrix}\begin{bmatrix}cos\gamma_y & 0 & sin\gamma_y\\ 0 & 1 & 0\\ -sin\gamma_y & 0 & cos\gamma_y\end{bmatrix}\begin{bmatrix}1 & 0 & 0\\ 0 & cos\gamma_x & -sin\gamma_x\\ 0 & sin\gamma_x & cos\gamma_x\end{bmatrix} \tag{7}$$

IEEE Transactions on Automation Science and Engineering (T-ASE) paper, presented at ICRA 2026, Vienna, Austria.

suitable error model, and the error model of Eq.(22) is improved to

$$\overline{\mathcal{M}} + \widetilde{\mathcal{M}} = (\mathcal{N} + \widetilde{\mathcal{N}})\mathcal{X} \tag{23}$$

where $\widetilde{\mathcal{N}}$ represents the error in the data matrix.

The TLS method uses orthogonal regression to account for noises and disturbances in forces/torques, velocities, and accelerations.

B. RRTLS Based Identification Method

With k sampled static data, the static identification equation Eq.(17) can be written as

$$^{S}\boldsymbol{F}_{raw,\Xi} = {}^{S}\boldsymbol{B}_{\Xi}{}^{S}\boldsymbol{\Psi} \tag{24}$$

where

$$\begin{aligned} {}^{S}\boldsymbol{F}_{raw,\Xi} &= [{}^{S}\boldsymbol{F}_{raw,1}, {}^{S}\boldsymbol{F}_{raw,2}, \ldots, {}^{S}\boldsymbol{F}_{raw,k}]^{T}, \\ {}^{S}\boldsymbol{B}_{\Xi} &= [{}^{S}\boldsymbol{B}_{1}.{}^{S}\boldsymbol{B}_{2}, \ldots {}^{S}\boldsymbol{B}_{k}]^{T} \end{aligned} \tag{25}$$

The subscript $_{\Xi}$ is omitted for brevity. The TLS solution of $^{S}\boldsymbol{\Psi}$ can be obtained as

$$\begin{aligned} {}^{S}\widehat{\boldsymbol{\Psi}} = \underset{{}^{S}\boldsymbol{\Psi}, {}^{S}\widehat{\boldsymbol{B}}, {}^{S}\widehat{\boldsymbol{F}}_{raw}}{argmin} & \left\| \left[{}^{S}\boldsymbol{B} \ {}^{S}\boldsymbol{F}_{raw} \right] - \left[{}^{S}\widehat{\boldsymbol{B}} \ {}^{S}\widehat{\boldsymbol{F}}_{raw} \right] \right\|_{\mathbf{F}} \\ subject \ to \quad & {}^{S}\widehat{F}_{raw} = {}^{S}\widehat{\boldsymbol{B}}\,{}^{S}\boldsymbol{\Psi} \end{aligned} \tag{26}$$

where $\|\cdot\|_{\mathbf{F}}$ indicates the Frobenius norm. Consider the singular value decomposition (SVD) of an augmented matrix Z containing all measured values.

$$Z = USV^{T}, where\ V \in \mathbb{R}^{q\times q}\ and\ S = (S_{1,1}, \ldots, S_{q,q}) \tag{27}$$

where Z represents the augmented matrix $\left[{}^{S}\widehat{\boldsymbol{B}} \ {}^{S}\widehat{\boldsymbol{F}}_{raw} \right]$.

The parameter vector $^{S}\widehat{\boldsymbol{\Psi}}$ is obtained as

$${}^{S}\widehat{\boldsymbol{\Psi}} = -\frac{v_{1:n}}{v_{q}}, \Delta Z = Z(vv^{T}) \tag{28}$$

where $v := V_{:,q}$ represents the smallest right singular vector and $V_{:,q}$ means last column of the matrix of eigenvectors V.

Moreover, the dynamic parameter identification model, that is, Eq.(4) can be written in the matrix form as

$${}^{S}\boldsymbol{F}_{nc\Xi} = {}^{S}\boldsymbol{A}_{\Xi}{}^{S}\boldsymbol{\Phi} \tag{29}$$

$$\begin{aligned} {}^{S}\boldsymbol{F}_{nc,\Xi} &= [{}^{S}\boldsymbol{F}_{nc,1}, {}^{S}\boldsymbol{F}_{nc,2}, \ldots, {}^{S}\boldsymbol{F}_{nc,k}]^{T}, \\ {}^{S}\boldsymbol{A}_{\Xi} &= [{}^{S}\boldsymbol{A}_{1}.{}^{S}\boldsymbol{A}_{2}, \ldots {}^{S}\boldsymbol{A}_{k}]^{T} \end{aligned} \tag{30}$$

For simplicity, the subscript $_{\Xi}$ is omitted for the rest of this section. Because of the high cost of SVD or SVD update, TLS is not flexible in dynamic parameter identification, which is an online estimation of a large number of data updates. Therefore, TLS methods for recursive computation need to be implemented. In [43], the RRTLS algorithm with low computational cost and suitable for online updating is proposed. This algorithm uses the one-step generalized inverse iteration to replace the generalized inverse iteration in the previous RTLS methods to track the minimum right singular vector. Table I presents the advantages and disadvantages of TLS-based methods to our identification problem.

TABLE I
ADVANTAGES AND DISADVANTAGES OF TLS-BASED METHODS

TLS	√ : The identification results were obtained by orthogonal regression based on all data matrices. × : The high cost of SVD and SVD updates makes it possible to calculate only offline
RTLS	√ : Based on incremental updating, the optimal solution is updated online through recursive calculation. × : Suboptimal recursive estimation requires a certain amount of data to converge to the optimal value.
RRTLS	√ : Based on RTLS, one-step generalized inverse iteration is used instead of generalized inverse iteration to track the minimum right singular vector. × : Suboptimal recursive estimation requires a certain amount of data to converge to the optimal value.

By modeling Eq.(29) as the following restricted TLS problem

$$\begin{aligned} {}^{S}\widehat{\boldsymbol{\Phi}} = & \underset{{}^{S}\boldsymbol{\Phi}, E}{argmin} \left\| H \right\|_{F} \\ & subject\ to \left[\mathcal{Z} + DWE^{T} \right] \begin{bmatrix} {}^{S}\boldsymbol{\Phi} \\ -1 \end{bmatrix} = 0 \end{aligned} \tag{31}$$

where $H \in R^{m\times p}$ is an arbitrary matrix. $\mathcal{Z}$ represents the augmented matrix $\left[{}^{S}\boldsymbol{A} \ {}^{S}\boldsymbol{F}_{nc} \right]$, $D \in R^{k\times m}$ and $E \in R^{(n+1)\times p}$ are full column rank matrices such that

$$P_{l} = DD^{T}, \quad P_{r} = EE^{T} \tag{32}$$

where P_l and P_l are the left and right noise covariance matrix respectively. Using the Lemma 2.2 introduced in [44], the problem Eq.(31) is equivalent to

$${}^{S}\widehat{\boldsymbol{\Phi}} = \underset{{}^{S}\boldsymbol{\Phi}}{argmin} \frac{{}^{S}\overline{\boldsymbol{\Phi}}^{T}\overline{\mathcal{Z}}^{T}P_{l}^{-1}\overline{\mathcal{Z}}{}^{S}\overline{\boldsymbol{\Phi}}}{{}^{S}\overline{\boldsymbol{\Phi}}^{T}\widehat{P}{}^{S}\overline{\boldsymbol{\Phi}}}, {}^{S}\overline{\boldsymbol{\Phi}} = [{}^{S}\boldsymbol{\Phi}^{T}, -1]^{T} \tag{33}$$

The one-step generalized inverse iteration in [45] will be used here to solve the Eq.(33) as

$$\begin{cases} \upsilon'_{k-1} = [{}^{S}\widehat{\boldsymbol{\Phi}}_{k-1}^{T}, -1]^{T} \\ \upsilon'_{k} = (\mathcal{Z}^{T}P_{r,k}^{-1}\mathcal{Z})^{-1}(P_{r,k}\upsilon'_{k-1}) = P_{k}(P_{r}\upsilon'_{k-1}) \\ {}^{S}\widehat{\boldsymbol{\Phi}}_{k} = -\upsilon'_{1:n;k}/\upsilon'_{(n+1);k} \end{cases} \tag{34}$$

where P_k represents the inverse of the data covariance matrix; n is the number of the parameters to be estimated; $\upsilon'_{1:n;k}$ denotes the sub-vector of υ'_{k} from the 1-th to the n-th element; with a forgetting factor λ_f, P_l can be constructed as $P_l = diag(\lambda_f^{k-1}, \lambda_f^{k-2}, \ldots, \lambda_f, 1)$.

Further, the recursive form of P_k^{-1} can be written as

$$\begin{cases} K_{k} = P_{k-1}\mathcal{Z}_{k}^{T}(\lambda_{f} + \mathcal{Z}_{k}P_{k-1}{}^{S}\widehat{\boldsymbol{\Phi}}_{k}^{T})^{-1} \\ P_{k} = \frac{1}{\lambda_{f}}(P_{k-1} - K_{k}\mathcal{Z}_{k}, P_{k-1}) \\ P_{k}^{-1} = \mathcal{Z}^{T}P_{l,k}^{-1}\mathcal{Z} = \sum_{i=1}^{k}\lambda_{f}^{k-i}\mathcal{Z}_{i}^{T}\mathcal{Z}_{i} = \lambda_{f}P_{k-1}^{-1} + \mathcal{Z}_{k}^{T}\mathcal{Z}_{k} \end{cases} \tag{35}$$

where $\mathcal{Z}_i$ represents the i-th row of $\mathcal{Z}$.

In addition, the initial values of some parameters in $^{S}\widehat{\boldsymbol{\Phi}}_{0}$ can be obtained from Eq.(28).

IEEE Transactions on Automation Science and Engineering (T-ASE) paper, presented at ICRA 2026, Vienna, Austria.

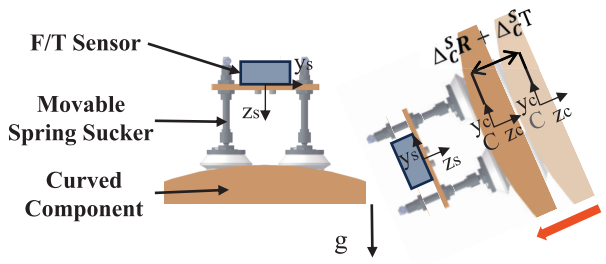

Fig. 2. When the angle between the direction of the workpiece and the direction of gravity is too large, the workpiece will rotate and shift using the movable spring sucker to absorb the curved component.

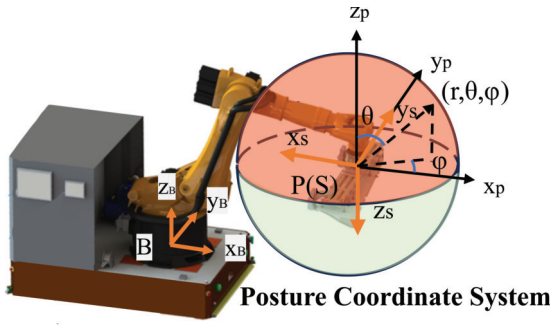

Fig. 3. Three axis vectors of {S} expressed in spherical coordinates are restricted to the feasible workspace.

IV. Identification Posture and Excitation Trajectory

In this section, a feasible workspace in posture coordinate system is established considering common industrial scenarios. On this basis, static identification postures and dynamic excitation trajectory are designed.

Due to the curvature of the surface of large components and the damage caused by mechanical gripping, large components are often adsorbed and gripped by movable spring suckers in industrial scenarios. Improper selection of posture in Fig. 2 will change the rotation ${}^{S}_{C}R$ and position ${}^{S}_{C}T$ of {C} relative to {S} during the identification process, leading to incorrect identification results.

Designing the identification postures and excitation trajectory not only needs to consider the validity of the postures and trajectory but also the feasibility and safety of the robot gripping the payload in the actual space. In order to limit the working postures of the robot, the posture coordinate system {P} of the robot is established as a spherical coordinate system with the center of {S} as the origin. The coordinate system direction of {P} is the same as that of {B}. The {S} in {P} is shown in Fig.3.

Let $(1,\phi_x,\theta_x),(1,\phi_y,\theta_y),(1,\phi_z,\theta_z)$ represent the ordered array of unit vectors of the three coordinate axes (x_s,y_s,z_s) of {S} in {P}. Then the cartesian coordinates of the sensor coordinate axes in {P} are expressed as

$$\begin{bmatrix} x_s \\ y_s \\ z_s \end{bmatrix} = \begin{bmatrix} sin\theta_x cos\phi_x & sin\theta_x sin\phi_x & cos\theta_x \\ sin\theta_y cos\phi_y & sin\theta_y sin\phi_y & cos\theta_y \\ sin\theta_z cos\phi_z & sin\theta_z sin\phi_z & cos\theta_z \end{bmatrix} \tag{36}$$

The three coordinate axis vectors of the {S} are visualized in two dimensions, as shown in Fig.4. The light green area is the feasible workspace of each axis in {P}, which can be adjusted according to the actual situation.

A. Identification Posture for Static Identification

The identification of the base inclination errors and zero-drift values in the static identification equation requires multiple measurement data in the static postures. Theoretically, with the increase of the measurement matrices, better identification results will be obtained, but more time will be consumed. Under the overall consideration of better optimization of identification results and avoidance of longer time, the desired postures acquisition method described by Algorithm 1 is designed.

Algorithm 1 GetTargetPosture

1 **procedure** GetTargetPosture(N_{target})
2 **for** each $n \in [1,+\infty]$ **do**
3 **for** each $i \in [0,n]$ **do**
4 $\gamma_z = 0 + \frac{2\pi}{n} i$
5 **for** each $j \in [0,n]$ **do**
6 $\gamma_y = 0 + \frac{\pi}{n} j$
7 $\gamma_x = \begin{cases} K\gamma_z & \text{if } 0 \leqslant \gamma_z < \pi \\ -K(2\pi-\gamma_z) & \text{if } \pi \leqslant \gamma_z \leqslant 2\pi \end{cases}$
8 $POS_{init} = {}^{B}_{S}R = R_Z(\gamma_z)R_Y(\gamma_y)R_X(\gamma_x)$
9 **if** $POS_{init} \in$ feasible workspace **then**
10 $POS_{target} = \left[POS_{target}\ POS_{init}\right]$
11 **end if**
12 **end for**
13 **end for**
14 **if** NUMBER(POS_{target}) > N_{target} **then**
15 **return:** POS_{target}
16 **end if**
17 **end for**

First, we enter the number of identification postures N_{target} we expect to obtain in line 1. Secondly, in lines 2-8, γ_z and γ_y in the Z-Y-X Euler angles $(\gamma_z,\gamma_y,\gamma_x)$ of {S} to {B} are equivalent divided in $[0,2\pi]$ and $[0,\pi]$, respectively. γ_x is set to different values according to the value of γ_z to obtain the symmetric identification posture in space, where K is adjustable. The identification postures POS_{init} of {S} evenly distributed in space is preliminarily obtained by Eq.(7). Then, the security judgment is made in lines 9-10, and the posture belonging to the set feasible workspace will be added to the identification posture matrix POS_{target}. In lines 14-16, if the number of postures NUMBER(POS_{target}) in the identification posture matrix is greater than N_{target}, the loop will be withdrawn and return POS_{target}. Note that if the components of the gravity vector in multiple postures are the same in {S}, the de-emphasis process will be performed.

B. Excitation Trajectory for Dynamic Identification

The unknown parameters in the dynamic identification equation can be identified by changing the posture of the robot.

IEEE Transactions on Automation Science and Engineering (T-ASE) paper, presented at ICRA 2026, Vienna, Austria.

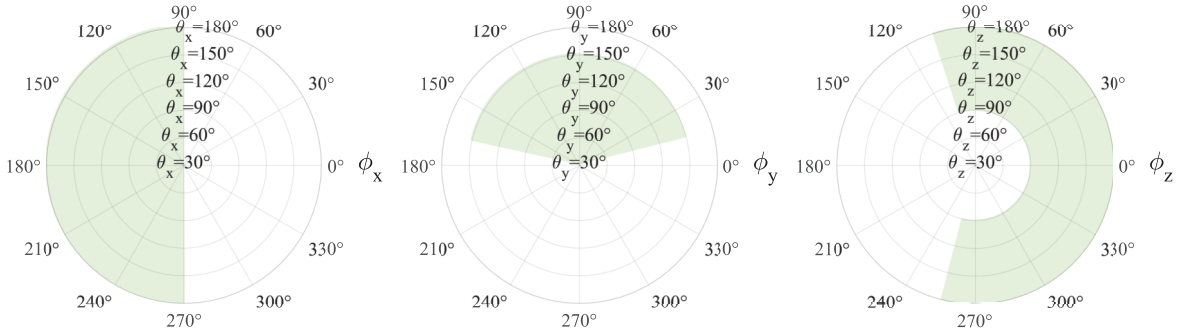

Fig. 4. A set restricted area represented by light green will act as the feasible workspace for {S} in {P}.

Due to the large components, we only change the robot's 4-6 joints to change the posture for safety. In order to make the selected postures represent the identification space as much as possible, it is necessary to design the optimal excitation trajectory. The non-contact inertial forces ${}^S\boldsymbol{f}_{iner}$ and torques ${}^S\boldsymbol{\tau}_{iner}$ without considering the influence of gravity are taken as the excitation equation, which can be obtained from Eq.(2)

$$\begin{bmatrix} {}^S\boldsymbol{f}_{iner} \\ {}^S\boldsymbol{\tau}_{iner} \end{bmatrix} = \begin{bmatrix} m{}^S\boldsymbol{a} + {}^S\boldsymbol{\alpha} \times m{}^S\boldsymbol{c} + {}^S\boldsymbol{\omega} \times ({}^S\boldsymbol{\omega} \times m{}^S\boldsymbol{c}) \\ {}^S\boldsymbol{I}{}^S\boldsymbol{\alpha} + {}^S\boldsymbol{\omega} \times ({}^S\boldsymbol{I}{}^S\boldsymbol{\omega}) + m{}^S\boldsymbol{c} \times {}^S\boldsymbol{a} \end{bmatrix} \tag{37}$$

The above formula can be reconfigured as

$${}^S\boldsymbol{F}_{iner} = {}^S\boldsymbol{C}({}^S\boldsymbol{a}, {}^S\boldsymbol{\alpha}, {}^S\boldsymbol{\omega}){}^S\boldsymbol{\Omega} \tag{38}$$

where ${}^S\boldsymbol{a}, {}^S\boldsymbol{\alpha}, {}^S\boldsymbol{\omega}$ in ${}^S\boldsymbol{C}$ are the function of the robot's 4-6 joints (q_4, q_5, q_6), denoted as ${}^S\boldsymbol{C} = f(q_4, q_5, q_6)$. The optimization objective function is denoted as $minf({}^S\boldsymbol{C})$. The correlation matrix Υ consists of M ${}^S\boldsymbol{C}$ matrices.

$$\Upsilon = {}^S\boldsymbol{C}_\Xi^T {}^S\boldsymbol{C}_\Xi, {}^S\boldsymbol{C}_\Xi = [{}^S\boldsymbol{C}_1^T {}^S\boldsymbol{C}_2^T \dots {}^S\boldsymbol{C}_M^T]^T \tag{39}$$

The condition number is introduced as the optimization objective function of the excitation trajectory.

$$minf({}^S\boldsymbol{C}) = Cond(\Upsilon) \tag{40}$$

The excitation trajectory of each joint is expressed as a Fourier series of finite terms, then the displacement q_i, velocity $\dot{q}_i$ and acceleration $\ddot{q}_i$ of the joint i can be expressed as

$$\begin{cases} q_i(t) = \sum_{l=1}^N \left[\frac{a_{i,l}}{\omega_f l} \sin(\omega_f l t) - \frac{b_{i,l}}{\omega_f l} \cos(\omega_f l t) \right] + q_{i,0} \\ \dot{q}_i(t) = \sum_{l=1}^N \left[a_{i,l} \cos(\omega_f l t) + b_{i,l} \sin(\omega_f l t) \right] \\ \ddot{q}_i(t) = \sum_{l=1}^N \omega_f l \left[-a_{i,l} \sin(\omega_f l t) + b_{i,l} \cos(\omega_f l t) \right] \end{cases} \tag{41}$$

where N is the number of sine and cosine. $a_{i,l}$ and $b_{i,l}$ are the weights of the sine and cosine parts respectively. $\omega_f = 2\pi f_f$ is the fundamental angular frequency. In order to satisfy the constraints of the robot joints, the constraint expression shown below is given

$$\begin{cases} |q_i(t)| \leqslant \left| \sum_{l=1}^N \frac{1}{\omega_f l} \sqrt{a_{i,l}^2 + b_{i,l}^2} + q_{i,0} \right| \leqslant q_{i,max} \\ |\dot{q}_i(t)| \leqslant \left| \sum_{l=1}^N \sqrt{a_{i,l}^2 + b_{i,l}^2} \right| \leqslant \dot{q}_{i,max} \\ |\ddot{q}_i(t)| \leqslant \left| \sum_{l=1}^N \omega_f l \sqrt{a_{i,l}^2 + b_{i,l}^2} \right| \leqslant \ddot{q}_{i,max} \\ pose = {}_S^B R = f_k(q_1, q_2, q_3, q_4, q_5, q_6) \\ \qquad \in feasible\ work\ space \end{cases} \tag{42}$$

where $f_k(q_1, q_2, q_3, q_4, q_5, q_6)$ on behalf of the transformation matrix is obtained by forward kinematics. The starting and ending constraint equations are

$$\begin{cases} q_i(t_0) = \sum_{l=1}^N \left(-\frac{b_{i,l}}{\omega_f l} \right) + q_{i,0} = q_{i,0} \\ \dot{q}_i(t_0) = \sum_{l=1}^N a_{i,l} = 0 \\ \ddot{q}_i(t_0) = \sum_{l=1}^N \omega_f l b_{i,l} = 0 \end{cases} \tag{43}$$

The optimization objective function and constraints are input into the *fmincon* function in MATLAB to obtain the excitation trajectory. By minimizing the value of the optimization objective function, the excitation trajectory can diversify the postures of the robot as much as possible under the above constraints [30], [34].

V. Experimental Results

In order to verify the proposed two-stage approach, a series of experiments are carried out in this section.

The assembly components of aircraft movable wings have high payload, high operation difficulty and complex assembly relationships. At present, crane or rack transportation is generally used, combined with manual processing to achieve assembly, which is strongly dependent on the level of operators. Through human-robot collaboration to improve assembly efficiency and reduce the load of operators can improve the flexibility of assembly requirements and adapt to the general trend of intelligent manufacturing. External force sensing is realized by parameter identification and compensation of payload, which provides the basis for human-robot collaborative assembly. The mobile human-robot collaborative assembly platform used to validate the optimization performance of the proposed parameter identification method is shown in Fig. 5.

A 6-DOF KUKA KR60HA (workspace radius 2033 mm, rated payload 60 kg) equipped with a 6-DOF force/torque ATI Omega160 (measuring range: ±2500 N on X-Y, ±6250 N on Z, ±400 Nm on all axes, effective resolution 1/2 N-1/20 Nm) is mounted on the mobile device. The kinematic parameters of the robot have been processed with error compensation [46]. The data measured by the force/torque sensor is filtered by moving mean for 10 sampling periods.

A. Identification Results of Inertial Parameters

The experiments are first carried out on a test payload component with a theoretical model to verify the effectiveness of the proposed method in parameter identification.

IEEE Transactions on Automation Science and Engineering (T-ASE) paper, presented at ICRA 2026, Vienna, Austria.

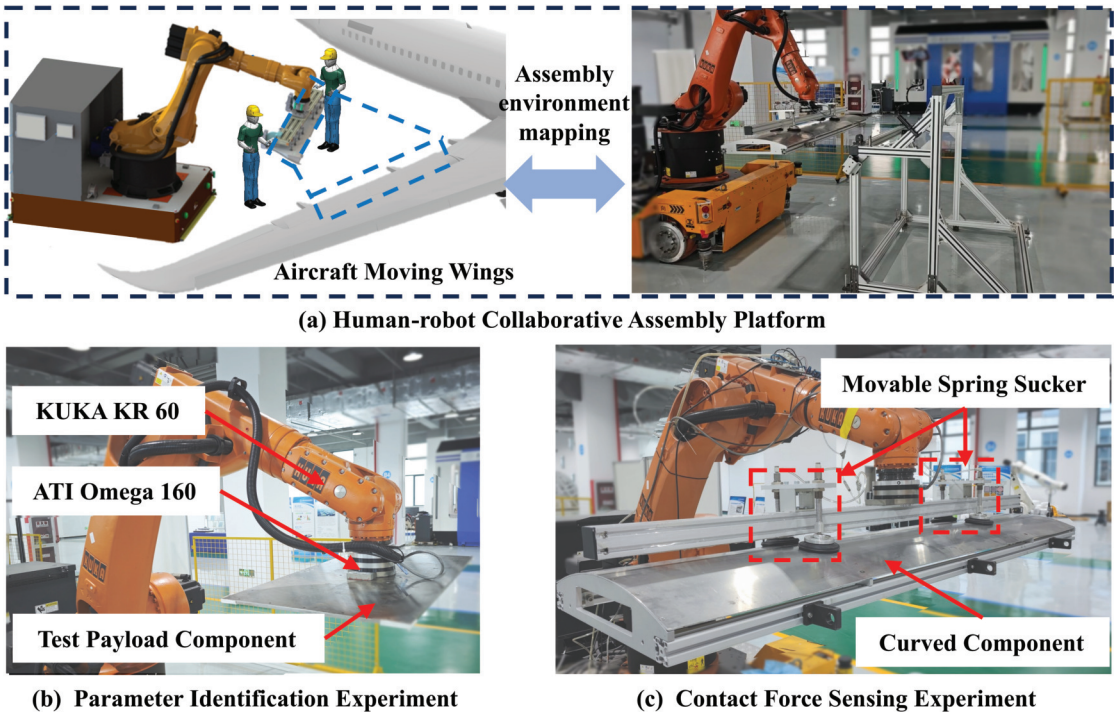

Fig. 5. Construct a human-robot collaborative assembly platform to simulate the assembly of aircraft moving wings (a). The robot is mounted on the automated guided vehicle with a 6-DOF force/torque sensor attached to the test payload component at the end-effector (b). The curved component used to simulate the aircraft moving wing is absorbed through the movable spring sucker (c).

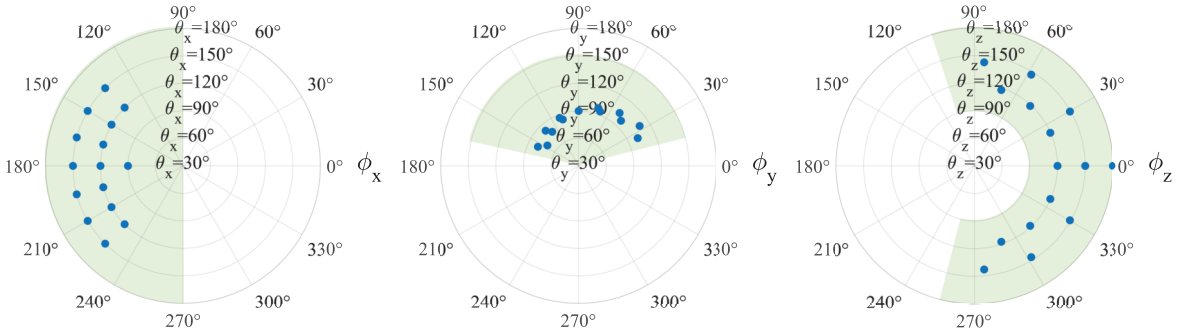

Fig. 6. Three axis vectors of {S} corresponding to the obtained static identification postures are represented in spherical coordinates, which satisfies the feasible workspace.

Set the number of identification postures N_{target} = 15, K = −0.2. By using the Algorithm 1, the Euler angles corresponding to the static identification postures can be obtained. The X, Y and Z axes of {S} corresponding to each identification posture are shown in Fig. 6, which satisfy the feasible workspace.

For the acquisition of excitation trajectory, the number of sine and cosine terms is taken as N =5, the fundamental frequency f_f is selected as 0.1 Hz, and the sampling frequency is taken as 250 Hz. The angles of the robot joints under the dynamic trajectories are shown in Fig. 7, and the corresponding axes of {S} are shown in Fig. 8, which meets the feasible workspace. Trajectory 1 is the excitation trajectory generated by the *fmincon* function, which is used for parameter dynamic identification. Trajectory 2 is designed as a random test trajectory to verify the external force/torque sensing results. Dynamic parameters are estimated at 250 Hz with an identification duration of 10 s. The time required for each identification posture is about 2 s and the calculation time can be ignored, so the entire identification process is 40 s. ${}^{S}\boldsymbol{a}$,${}^{S}\boldsymbol{\alpha}$ and ${}^{S}\boldsymbol{\omega}$ are estimated online by Kalman filter [47]. The whole identification process is shown in Fig. 9.

In order to prove the optimization effect of the proposed method in parameter identification, two groups of common methods are designed as control tests:

- Method1 (static with TLS): The TLS method is used to identify the static equation, and the influence of inertial force/torque caused by rotation is ignored in the identification process and results.
- Method2 (dynamic with RTLS): The RTLS method is used to identify dynamic equations. This method ignores the influence of base inclination errors in the identification process and results.

IEEE Transactions on Automation Science and Engineering (T-ASE) paper, presented at ICRA 2026, Vienna, Austria.

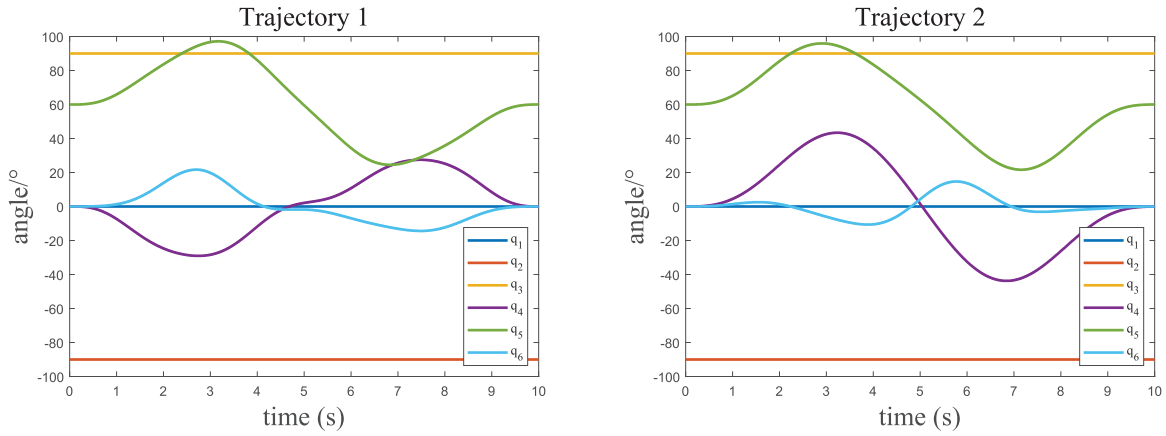

Fig. 7. Trajectory 1: excitation trajectory; Trajectory 2: random test trajectory.

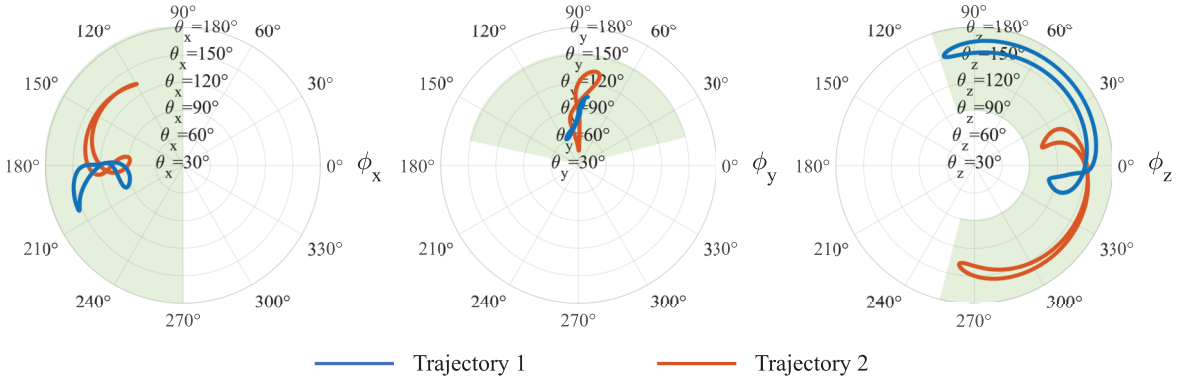

Fig. 8. Three axis vectors of {S} corresponding to the dynamic trajectories are represented in spherical coordinates, which satisfies the feasible workspace.

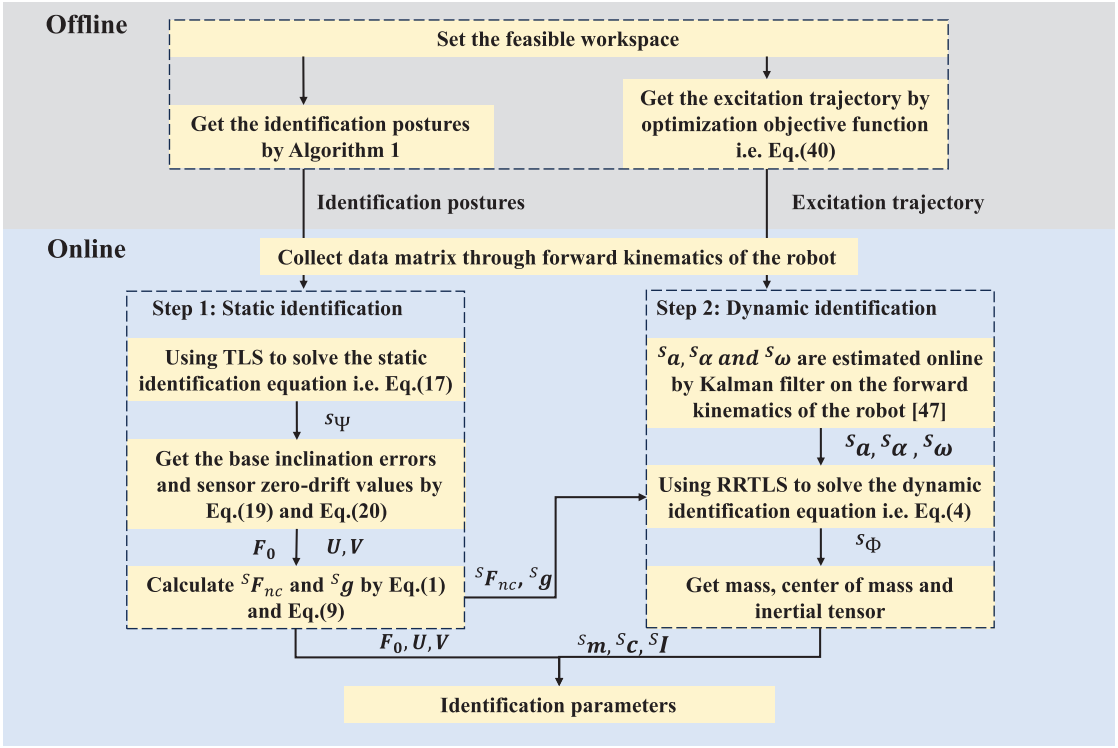

Fig. 9. Flow chart of the proposed parameter identification method.

IEEE Transactions on Automation Science and Engineering (T-ASE) paper, presented at ICRA 2026, Vienna, Austria.

TABLE II
A COMPARISON BETWEEN TLS, RTLS AND PROPOSED METHOD

Scenario 1	Reference	Method1	Error	Method2	Error	Proposed method	Error
m(kg)	40.173	40.542	0.370	40.098	0.075	40.164	$9.3 \cdot 10^{-3}$
mc_x(kg· m)	0	0.144	0.144	$-6.97 \cdot 10^{-3}$	$6.97 \cdot 10^{-3}$	$5.69 \cdot 10^{-3}$	$5.69 \cdot 10^{-3}$
mc_y(kg· m)	0	-0.135	0.135	$1.14 \cdot 10^{-2}$	$1.14 \cdot 10^{-2}$	$-8.38 \cdot 10^{-3}$	$8.38 \cdot 10^{-3}$
mc_z(kg· m)	0.905	1.053	0.148	0.853	0.052	0.893	0.012
I_{xx}(Nm)	3.24	/	/	3.453	0.213	3.205	0.035
I_{yy}(Nm)	0.809	/	/	0.837	0.028	0.833	0.024
I_{zz}(Nm)	4.049	/	/	4.176	0.127	4.013	0.036
U(°)	/	2.642	/	/	/	1.824	/
V(°)	/	-4.943	/	/	/	2.326	/

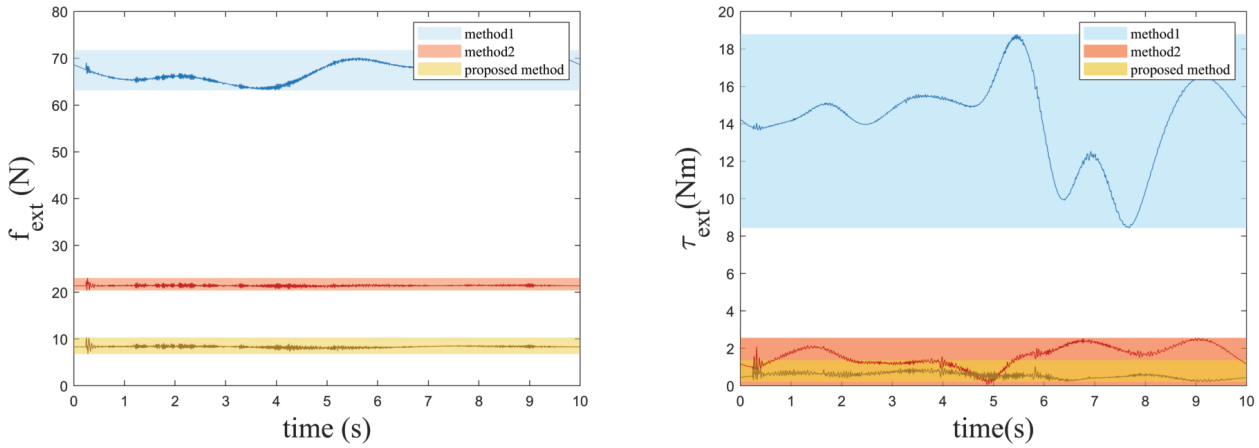

Fig. 10. Combined forces/torques f_{ext}/τ_{ext} of the three methods after compensated under high-speed test trajectory (The shaded parts represent their maximum and minimum value intervals).

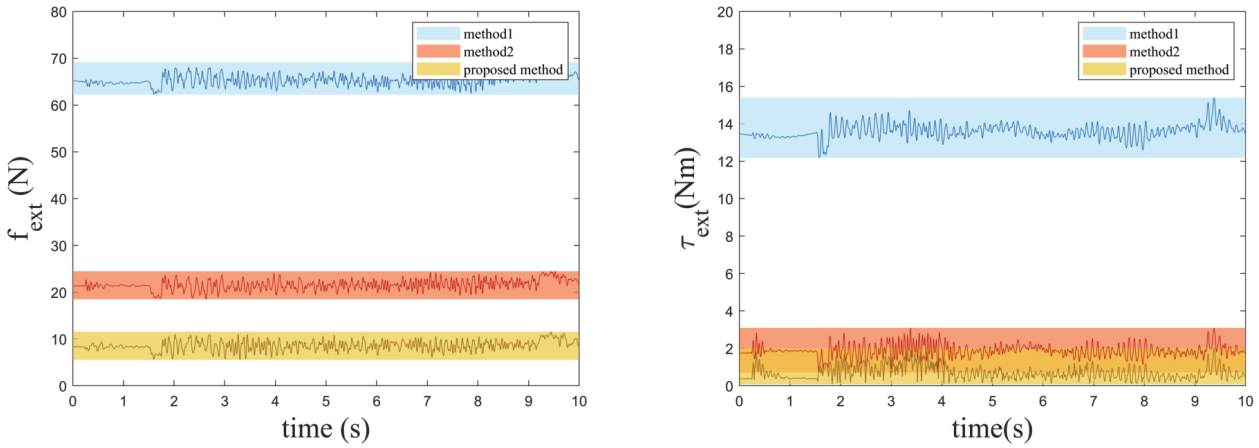

Fig. 11. Combined forces/torques f_{ext}/τ_{ext} of the three methods after compensated under low-speed test trajectory (The shaded parts represent their maximum and minimum value intervals).

The identification results and absolute errors of the three methods are shown in table II. It can be seen that the proposed method obtains better identification results on non-zero elements.

B. Experiments for Contact Force/Torque Sensing in Absence of Contact

In order to verify the effectiveness of the proposed method in industrial scenarios with high payloads and large dimensions, movable spring suckers are added to absorb the curved component to simulate the adsorption gripping tasks for random positions, with a payload of about 35 kg. In order to represent the change of external forces/torques, let f_{ext} and τ_{ext} denote the combined forces and torques of the external contact forces/torques, respectively.

We designed two sets of test trajectories to verify the effectiveness of the proposed method at high and low speeds. The high-speed test trajectory is trajectory 2 in Fig. 7, and the compensation result is shown in Fig. 10. Then, we used the interaction control scheme in [47] to capture the trajectory of

IEEE Transactions on Automation Science and Engineering (T-ASE) paper, presented at ICRA 2026, Vienna, Austria.

TABLE III
THE RESULT AFTER COMPENSATION UNDER TWO TEST TRAJECTORIES

Method	high-speed test trajectory					
	$f_{ext,t=0}$	Ave(f_{ext})	STDEV(f_{ext})	$\tau_{ext,t=0}$	Ave(τ_{ext})	STDEV(τ_{ext})
Method1	68.57	67.34	2.17	14.21	14.18	2.22
Method2	21.46	21.41	0.20	1.18	1.59	0.53
Proposed method	8.36	8.33	0.24	0.45	0.55	0.17
	low-speed test trajectory					
Method1	65.11	65.38	1.21	13.45	13.60	0.39
Method2	21.36	21.58	1.06	1.73	1.87	0.33
Proposed method	8.33	8.60	1.04	0.35	0.70	0.35

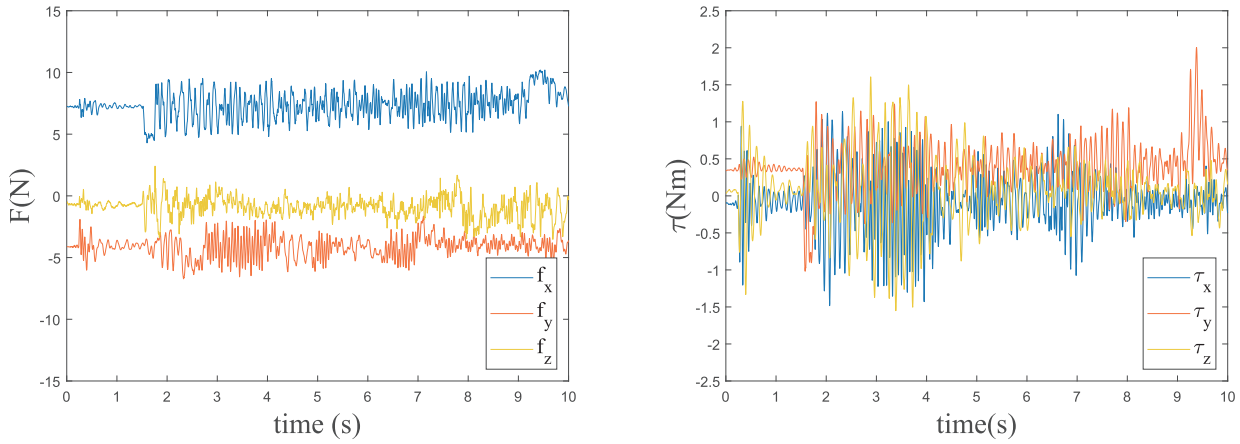

Fig. 12. Forces/torques after compensation by proposed method.

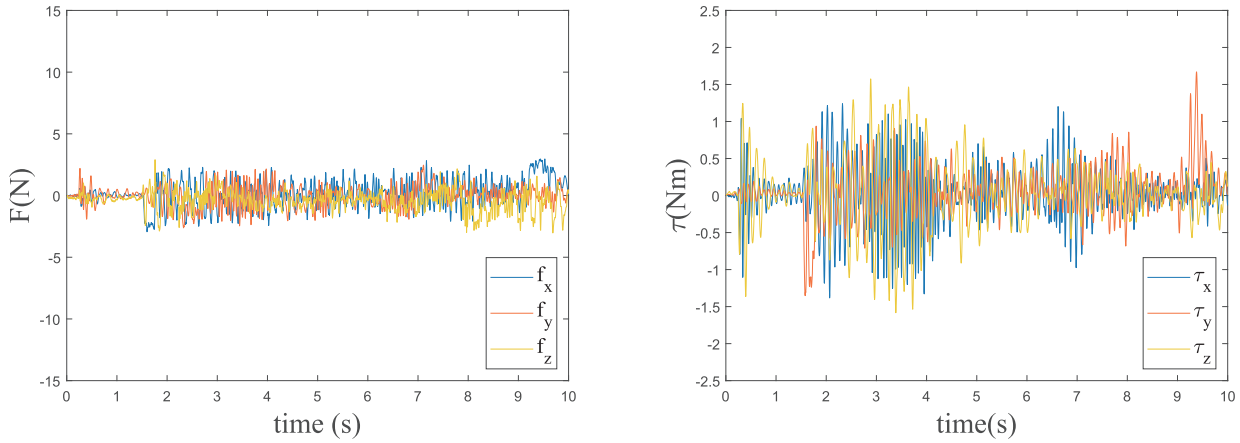

Fig. 13. Forces/torques after secondary zero-drift compensation by proposed method.

the operator's pulling the curved component for 10 s. Then, the collected operator's trajectory is used as the low-speed test trajectory, and the compensated values are shown in Fig. 11.

Table III lists the static initial values, mean values, and standard deviations of the external forces/torques after the three methods are compensated under the two trajectories. In the Method1, the influence of inertia forces/torques caused by rotation is ignored in the identification process and results, resulting in the external forces/torques being much larger than the other two methods in each index. Method2 and the proposed method consider the effect of inertia forces/torques caused by rotation, so as to obtain some optimization in the external forces/torques. Furthermore, the proposed method takes into account the influence of base inclination errors, thus obtaining a better external force/torque sensing result at high and low speeds than the previous two methods.

C. Secondary Zero-Drift Compensation

Taking human-robot collaboration as an example, the application of this method in low-speed motion needs to be further optimized. We take the external force/torque of each axis at the initial time as the reference value and carry out the secondary zero-drift compensation. Secondary zero-drift compensation is shown as

$$F'_{ext} = F_{ext} - F_{ext,t=0} \tag{44}$$

IEEE Transactions on Automation Science and Engineering (T-ASE) paper, presented at ICRA 2026, Vienna, Austria.

where F'_{ext} represents the external forces/torques after secondary zero-drift compensation. $F_{ext,t=0}$ represents the initial external forces/torques after the initial compensation. The external forces/torques of each axis after the initial compensation under the low-speed test trajectory of the proposed method are shown in Fig. 12, and the external forces/torques after the secondary zero-drift compensation are shown in Fig. 13. The maximum absolute compensated force and torque of the proposed method are 3.03 N and 1.67 Nm, respectively. It can be seen that the method proposed in this paper can be applicable to tasks with large sizes and high payloads in industrial scenarios.

VI. Conclusion

Inadequate error source consideration or inappropriate identification model can have an impact on payload identification and diminish the accuracy of contact force sensing, especially for large components. In this paper, a two-stage payload dynamic parameter identification method is proposed. The two-stage parameter identification equation is developed to investigate the relationship between the parameters to be identified and the measured forces/torques of the sensor. A parameter identification model based on the TLS variable error model that explicitly takes into account the errors of all relevant variables is developed, together with a flexible RRTLS algorithm suitable for online updating. Considering the feasibility and safety of the robot's working postures, a feasible workspace under the posture coordinate system is established. On this basis, the static identification postures and the optimized excitation trajectory are designed to realize the identification of payload parameters.

The external contact force sensing errors of high payload under high-speed and low-speed test trajectories show the effectiveness of the proposed method. Further, the application of secondary zero-drift compensation shows the potential of contact force sensing in, but not limited to, human-robot collaboration applications. We aim to accurately obtain the contact forces for large components by using the proposed parameter identification method. In future work, we will focus on the practical implementation of contact operations such as human-robot collaborative assembly in high-payload industrial scenarios.

References

[1] C. J. Conti, A. S. Varde, and W. Wang, "Human–robot collaboration with commonsense reasoning in smart manufacturing contexts," *IEEE Trans. Autom. Sci. Eng.*, vol. 19, no. 3, pp. 1784–1797, Jul. 2022.

[2] N. Lucci, A. Monguzzi, A. M. Zanchettin, and P. Rocco, "Workflow modelling for human–robot collaborative assembly operations," *Robot. Comput.-Integr. Manuf.*, vol. 78, Dec. 2022, Art. no. 102384.

[3] M. H. Raibert and J. J. Craig, "Hybrid position/force control of manipulators," *J. Dyn. Syst. Meas. Control*, vol. 103, no. 2, pp. 126–133, Jun. 1981.

[4] H. Neville, "Impedance control: An approach to manipulation: Part I-theory," *J. Dyn. Syst. Meas. Control*, vol. 107, no. 1, pp. 1–7, Mar. 1985.

[5] A. Q. Keemink, H. van der Kooij, and A. H. Stienen, "Admittance control for physical human–robot interaction," *Int. J. Robot. Res.*, vol. 37, no. 11, pp. 1421–1444, 2018.

[6] E. Magrini, F. Ferraguti, A. J. Ronga, F. Pini, A. De Luca, and F. Leali, "Human–robot coexistence and interaction in open industrial cells," *Robot. Comput.-Integr. Manuf.*, vol. 61, Feb. 2020, Art. no. 101846.

[7] C. Gosselin et al., "A friendly beast of burden: A human-assistive robot for handling large payloads," *IEEE Robot. Autom. Mag.*, vol. 20, no. 4, pp. 139–147, Dec. 2013.

[8] A. Sidiropoulos et al., "Safe and effective collaboration with a high-payload robot: A framework integrating novel hardware and software modules," *IEEE Robot. Autom. Mag.*, vol. 31, no. 3, pp. 38–47, Mar. 2024.

[9] P. Franceschi, D. Cassinelli, N. Pedrocchi, M. Beschi, and P. Rocco, "Design of an assistive controller for physical human–robot interaction based on cooperative game theory and human intention estimation," *IEEE Trans. Autom. Sci. Eng.*, vol. 22, pp. 5741–5756, 2024.

[10] S. Zhang, S. Wang, F. Jing, and M. Tan, "A sensorless hand guiding scheme based on model identification and control for industrial robot," *IEEE Trans. Ind. Informat.*, vol. 15, no. 9, pp. 5204–5213, Sep. 2019.

[11] Y. Lu, Z. Shen, H. Hu, C. Zhuang, and H. Ding, "A unified framework of in-situ calibration and synchronous identification for industrial robots using composite sensing," *IEEE Trans. Autom. Sci. Eng.*, vol. 22, pp. 1405–1424, 2025.

[12] Y. Wei, S. Lyu, W. Li, X. Yu, Z. Wang, and L. Guo, "Contact force estimation of robot manipulators with imperfect dynamic model: On Gaussian process adaptive disturbance Kalman filter," *IEEE Trans. Autom. Sci. Eng.*, vol. 21, no. 3, pp. 3524–3537, Mar. 2024.

[13] L. Dinh Phong, J. Choi, and S. Kang, "External force estimation using joint torque sensors for a robot manipulator," in *Proc. IEEE Int. Conf. Robot. Autom.*, May 2012, pp. 4507–4512.

[14] X. Liu, F. Zhao, S. S. Ge, Y. Wu, and X. Mei, "End-effector force estimation for flexible-joint robots with global friction approximation using neural networks," *IEEE Trans. Ind. Informat.*, vol. 15, no. 3, pp. 1730–1741, Mar. 2019.

[15] G. Sebastian, Z. Li, V. Crocher, D. Kremers, Y. Tan, and D. Oetomo, "Interaction force estimation using extended state observers: An application to impedance-based assistive and rehabilitation robotics," *IEEE Robot. Automa. Lett.*, vol. 4, no. 2, pp. 1156–1161, Dec. 2019.

[16] B. Yao, Z. Zhou, L. Wang, W. Xu, Q. Liu, and A. Liu, "Sensorless and adaptive admittance control of industrial robot in physical human–robot interaction," *Robot. Comput.-Integr. Manuf.*, vol. 51, pp. 158–168, Dec. 2017.

[17] A. Wahrburg, J. Bos, K. D. Listmann, F. Dai, B. Matthias, and H. Ding, "Motor-current-based estimation of Cartesian contact forces and torques for robotic manipulators and its application to force control," *IEEE Trans. Autom. Sci. Eng.* , vol. 15, no. 2, pp. 879–886, Apr. 2018.

[18] A. Albu-Schäffer, S. Haddadin, C. Ott, A. Stemmer, T. Wimbock, and G. Hirzinger, "The DLR lightweight robot: Design and control concepts for robots in human environments," *Ind. Robot, Int. J.*, vol. 34, no. 5, pp. 376–385, Aug. 2007.

[19] W. Taie, K. ElGeneidy, A. Al-Yacoub, and S. Ronglei, "Online identification of payload inertial parameters using ensemble learning for collaborative robots," *IEEE Robot. Autom. Lett.*, vol. 9, no. 2, pp. 1350–1356, Feb. 2024.

[20] S. Liu, L. Wang, and X. V. Wang, "Sensorless force estimation for industrial robots using disturbance observer and neural learning of friction approximation," *Robot. Comput.-Integr. Manuf.*, vol. 71, Oct. 2021, Art. no. 102168.

[21] J. Swevers, W. Verdonck, B. Naumer, S. Pieters, and E. Biber, "An experimental robot load identification method for industrial application," *Int. J. Robot. Res.*, vol. 21, no. 8, pp. 701–712, Aug. 2002.

[22] Y. Sun, Y. Liu, T. Zou, M. Jin, and H. Liu, "Design and optimization of a novel six-axis force/torque sensor for space robot," *Measurement*, vol. 65, pp. 135–148, Apr. 2015.

[23] B. Shi, F. Wang, Z. Huo, Y. Tian, R. Cong, and D. Zhang, "Contact force sensing and control for inserting operation during precise assembly using a micromanipulator integrated with force sensors," *IEEE Trans. Autom. Sci. Eng.*, vol. 20, no. 3, pp. 2147–2155, Jul. 2023.

[24] D. Kubus, T. Kroger, and F. M. Wahl, "Improving force control performance by computational elimination of non-contact forces/torques," in *Proc. IEEE Int. Conf. Robot. Autom.*, May 2008, pp. 2617–2622.

[25] G. Bätz, B. Weber, M. Scheint, D. Wollherr, and M. Buss, "Dynamic contact force/torque observer: Sensor fusion for improved interaction control," *Int. J. Robot. Res.*, vol. 32, no. 4, pp. 446–457, Apr. 2013.

[26] F. Aghili, "Robust impedance control of manipulators carrying a heavy payload," *J. Dyn. Syst., Meas., Control*, vol. 132, no. 5, Sep. 2010, Art. no. 051011.

[27] S. G. Vougioukas, "Bias estimation and gravity compensation for force-torque sensors," in *Proc. Int. Conf. Math. Methods Comput. Techn. Electr. Eng.*, 2001, pp. 1–4.

IEEE Transactions on Automation Science and Engineering (T-ASE) paper, presented at ICRA 2026, Vienna, Austria.

[28] H. Zhang, L. Li, J. Zhao, and J. Zhao, "The hybrid force/position anti-disturbance control strategy for robot abrasive belt grinding of aviation blade base on fuzzy PID control," *Int. J. Adv. Manuf. Technol.*, vol. 114, nos. 11–12, pp. 3645–3656, Jun. 2021.

[29] K. Min, F. Ni, and H. Liu, "An efficient and accurate force/torque sensing method based on an excitation trajectory," *Ind. Robot, Int. J. Robot. Res. Appl.*, Feb. 2023.

[30] J. Duan, Z. Liu, Y. Bin, K. Cui, and Z. Dai, "Payload identification and gravity/inertial compensation for six-dimensional force/torque sensor with a fast and robust trajectory design approach," *Sensors*, vol. 22, no. 2, p. 439, Jan. 2022.

[31] S. Farsoni, F. Ferraguti, and M. Bonfè, "Safety-oriented robot payload identification using collision-free path planning and decoupling motions," *Robot. Comput.-Integr. Manuf.*, vol. 59, pp. 189–200, Oct. 2019.

[32] M. Tang, Y. Yan, B. An, W. Wang, and Y. Zhang, "Dynamic parameter identification of collaborative robot based on WLS-RWPSO algorithm," *Machines*, vol. 11, no. 2, p. 316, Feb. 2023.

[33] T. Xu, J. Fan, Q. Fang, Y. Zhu, and J. Zhao, "An accurate identification method based on double weighting for inertial parameters of robot payloads," *Robotica*, vol. 40, no. 12, pp. 4358–4374, Dec. 2022.

[34] D. Kubus, T. Kroger, and F. M. Wahl, "On-line estimation of inertial parameters using a recursive total least-squares approach," in *Proc. IEEE/RSJ Int. Conf. Intell. Robots Syst.*, Sep. 2008, pp. 3845–3852.

[35] S. Farsoni, C. T. Landi, F. Ferraguti, C. Secchi, and M. Bonfè, "Real-time identification of robot payload using a multirate quaternion-based Kalman filter and recursive total least-squares," in *Proc. IEEE Int. Conf. Robot. Autom. (ICRA)*, May 2018, pp. 2103–2109.

[36] T. Xu et al., "An online payload identification method based on parameter difference for industrial robots," *Robotica*, vol. 42, no. 8, pp. 2690–2712, Aug. 2024.

[37] Y. Yu, R. Shi, and Y. Lou, "Bias estimation and gravity compensation for wrist-mounted force/torque sensor," *IEEE Sensors J.*, vol. 22, no. 18, pp. 17625–17634, Sep. 2022.

[38] C. G. Atkeson, C. H. An, and J. M. Hollerbach, "Estimation of inertial parameters of manipulator loads and links," *Int. J. Robot. Res.*, vol. 5, no. 3, pp. 101–119, Sep. 1986.

[39] J. Swevers, C. Ganseman, D. B. Tukel, J. de Schutter, and H. Van Brussel, "Optimal robot excitation and identification," *IEEE Trans. Robot. Autom.*, vol. 13, no. 5, pp. 730–740, May 1997.

[40] J. Jin and N. Gans, "Parameter identification for industrial robots with a fast and robust trajectory design approach," *Robot. Comput.-Integr. Manuf.*, vol. 31, pp. 21–29, Feb. 2015.

[41] K. Kozlowski, *Modelling and Identification in Robotics*. Cham, Switzerland: Springer, 1998.

[42] D. Kubus, T. Kroger, and F. M. Wahl, "On-line rigid object recognition and pose estimation based on inertial parameters," in *Proc. IEEE/RSJ Int. Conf. Intell. Robots Syst.*, Oct. 2007, pp. 1402–1408.

[43] S. Rhode, K. Usevich, I. Markovsky, and F. Gauterin, "A recursive restricted total least-squares algorithm," *IEEE Trans. Signal Process.*, vol. 62, no. 21, pp. 5652–5662, Nov. 2014.

[44] A. Beck, "The matrix-restricted total least-squares problem," *Signal Process.*, vol. 87, no. 10, pp. 2303–2312, Oct. 2007.

[45] D.-Z. Feng and W. X. Zheng, "Fast approximate inverse power iteration algorithm for adaptive total least-squares FIR filtering," *IEEE Trans. Signal Process.*, vol. 54, no. 10, pp. 4032–4039, Oct. 2006.

[46] W. Wang, W. Tian, W. Liao, B. Li, and J. Hu, "Error compensation of industrial robot based on deep belief network and error similarity," *Robot. Comput.-Integr. Manuf.*, vol. 73, Feb. 2022, Art. no. 102220.

[47] S. Farsoni, C. T. Landi, F. Ferraguti, C. Secchi, and M. Bonfè, "Compensation of load dynamics for admittance controlled interactive industrial robots using a quaternion-based Kalman filter," *IEEE Robot. Autom. Lett.*, vol. 2, no. 2, pp. 672–679, Apr. 2017.